Journal of Alloys and Compounds 735 (2018) 1389–1394

Contents lists available at ScienceDirect

Journal of Alloys and Compounds

journal homepage: http://www.elsevier.com/locate/jalcom

A multiscale architectured CuCrZr alloy with high strength, electrical conductivity and thermal stability

Ningning Liang [a], Jizi Liu [a, b, *], Sicong Lin [a], Yue Wang [a], Jing Tao Wang [a, **], Yonghao Zhao [a], Yuntian Zhu [a, c]

[a] School of Materials Science and Engineering, Nanjing University of Science and Technology, Jiangsu 210094, China
[b] Herbert Gleiter Institute of Nanoscience, Nanjing University of Science and Technology, Jiangsu 210094, China
[c] Department of Materials Science and Engineering, North Carolina State University, Raleigh, NC 27695, USA

ARTICLE INFO

Article history:
Received 30 August 2017
Received in revised form
14 November 2017
Accepted 27 November 2017
Available online 28 November 2017

Keywords:
Copper alloy
ECAP
Ultrafine grains
Nanoscale twins
Precipitates

ABSTRACT

A multiscale architectured structure, nanotwinned ultrafine grains surrounded by nano-precipitates at grain boundaries, was developed in a bulk Cu-Cr-Zr alloy prepared by aging treatment following equal-channel angular pressing. A superior combination of high strength, high electrical conductivity and good thermal stability was obtained, which avoided the trade-off among these important properties of electric conductive materials. This provides insight understanding on the mechanisms for strengthening, thermal stability and electrical conductivity, and could help the development of high-performance electrical conductors.

1. Introduction

As a promising engineering material for contact wires for high-speed railways, CuCrZr alloys need more attractive combination of ultimate tensile strength (UTS), electrical conductivity and thermal stability to endure the service conditions of high-speed trains [1–3]. However, high strength and high electrical conductivity are often mutually exclusive in materials strengthened by conventional methods, such as alloying, strain hardening, or grain refinement [4–6]. During the last decade, materials with nanostructures, such as nano-precipitates [7,8], nanotwins [6,9,10], nanograins [11–13] etc., are extensively investigated for high strength and high conductivity. By introducing these nanostructures, some incompatible properties can be reached simultaneously. For example, nano-particles precipitated from alloy matrix has been reported to produce higher electrical conductivity and at the same time higher strength [14]. It was recently discovered that nanoscale twins led to a very high tensile strength and a considerable electrical conductivity for pure Cu and Cu-Cr-Zr alloys [15–17]. Also, with nanotwins, metals and alloys exhibit enhanced strength-ductility synergy [6]. In order to introduce these nanostructures into metals or alloys, many approaches have been attempted, such as pulsed electrodeposition [15], dynamic plastic deformation (DPD) [16], cryo-rolling [18], aging implemented after severe plastic deformations [14], and so on. Although the expected high strength and high electrical conductivity have been reached, the low thermal stability is still a limitation for practical applications [6]. By equal-channel angular pressing (ECAP) and aging, a bulk nanostructured Cu-Cr-Zr alloy was reported to have a tensile strength of 700 ± 40 MPa, an electrical conductivity of 77% IACS (International Annealed Copper Standard), and even good stability at elevated temperatures and under cyclic loading [13,14,19–21]. The strength and electrical conductivity are comparable to those of DPD-processed samples strengthened by nanotwins and nanograins [17], however, the strengthening mechanism in aged ECAP-processed samples was roughly attributed to strain hardening and precipitation strengthening. Obviously, the explanation is not convincingly, more study is needed to understand the outstanding combination of properties.

In this work, we carefully examine the microstructures in aged ECAP-samples, and focus on the understanding special

* Corresponding author. School of Materials Science and Engineering, Nanjing University of Science and Technology, Jiangsu 210094, China.
** Corresponding author.
E-mail addresses: jzliu@njust.edu.cn (J. Liu), jtwang@njust.edu.cn (J.T. Wang).

https://doi.org/10.1016/j.jallcom.2017.11.309
0925-8388/

microstructure features responsible for the good comprehensive properties of high strength, high electrical conductivity and thermal stability.

2. Experimental section

A Cu-0.45Cr-0.12Zr alloy was made by melting pure metals in appropriate weight ratios. The cast ingots were forged into bars with a dimension of 11.5 × 11.5 × 125 mm. Prior to ECAP, bars were homogenized in an air circulated furnace at 1000 °C for 2 h followed by water quenching. Optical microscopy shows that the as-homogenized specimens has an average grain size of ~500 μm. ECAP was performed with 0.4 mm/s velocity at room temperature via the so-called "route B_c" in a 90°die [22], which leads to an imposed strain of about 1.0 per pass. The ECAP process was carried out for 8 passes, after which the grains cannot be further refined and mechanical property would not be further improved [14]. The ECAP-processed samples were subsequently aged at different temperatures for a certain period of time in muffle furnace followed by air quenching, which is aimed to optimize the precipitation of Cr particles and test the thermal stability.

Vickers microhardness was measured on a HMV-G 21DT Micro Vickers Hardness Tester with an applied load of 100 g and a holding time of 10 s. The electrical conductivity was measured relative to the IACS by using a D60K-1201 digital conductivity meter. Both hardness and electrical conductivity were obtained by averaging at least five successive measurements. The tensile experiments were performed on a Shimadzu AGS-X universal tester with a constant strain rate of 10^{-3} s^{-1}. The dog-bone-shaped specimens used in the tensile tests were shaped by spark erosion to have a nearly rectangular cross-section of 3 × 2 mm^2 and a gauge length of 10 mm. The specimen axis was aligned with the direction of extrusion. An FEI Titan G2 60-300 transmission electron microscope (TEM) with a spherical aberration corrector under the objective lens operated at 300 kV was used to characterize the microstructures. The thin foil for TEM was sectioned from the plane perpendicular to the working axis.

3. Results

Fig. 1a shows the hardness and grain size of samples after ECAP and aging at different temperature for the same time (1 h). It was found that grain coarsening began when the ECAP-processed sample was isothermally annealed above 500 °C (for a duration of 1 h). At the same time, the hardness of the sample dropped rapidly. In other word, the temperature T_h, at which the maximum H_v was achieved, is close to 500 °C for 8-pass ECAP-processed specimens. The aging temperature was designed to be 460 °C. Fig. 1b shows the hardness and electrical conductivity of samples after ECAP and aging at 460 °C for different times. It is clear that the electrical conductivity increased with longer aging time, due to solute atoms aggregation and defects reduction. This increasing trend is especially apparent for the first hour. The hardness reached the peak value of 219 HV at 1.5 h and then decreased slowly.

Fig. 2 shows typical tensile stress-strain curves of the ECAP-processed and aged samples and the specific performance data for the tensile samples. The peak-aged samples have the highest tensile strength 676 MPa and the electrical conductivity of 73% IACS, which is close to the industry requirement of 75% IACS. The over-aged samples have higher electrical conductivity of 78.1% IACS and lower tensile strength of 612 MPa. Compared with the best combination of a tensile strength of 700 MPa and an electrical conductivity of 77% IACS, reported by Vinogradov [14], the drop of strength is mainly due to the larger average grain size of 256 nm in this study than that of 160 nm in Ref. [14], caused by lower Zr content and ECAP-pass number.

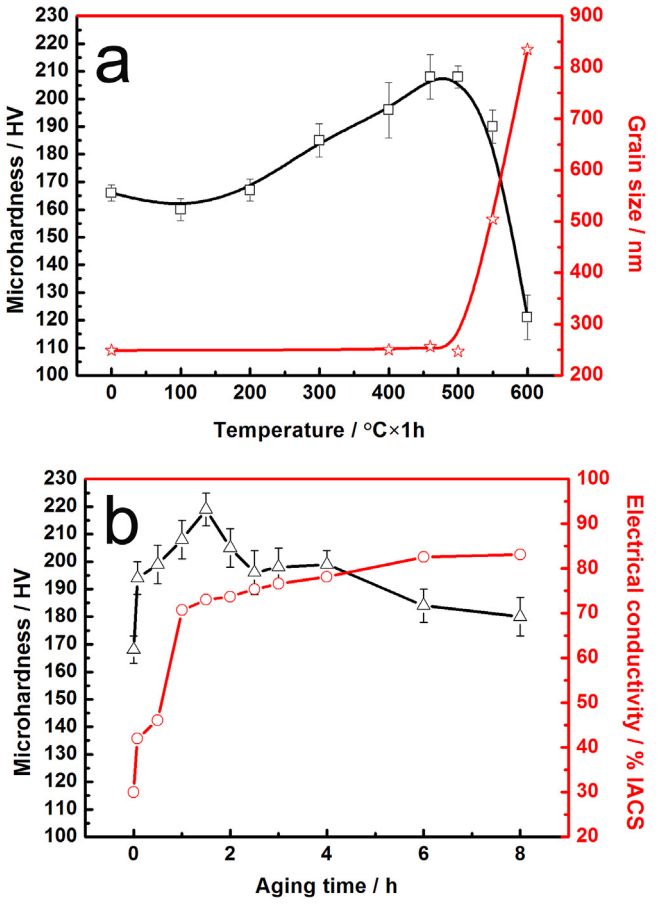

Fig. 1. Properties of CuCrZr alloy samples: (a) variations of hardness and grain size with aging temperature. The aging time is 1 h; (b) variations of hardness and electrical conductivity with aging time. The aging temperature is 460 °C.

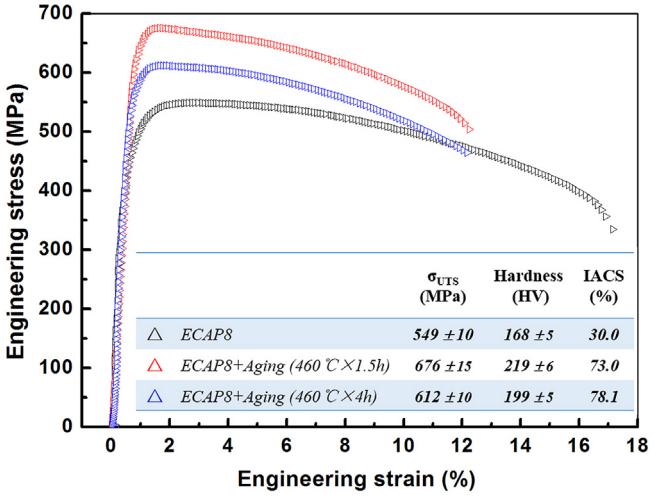

Fig. 2. Typical tensile stress-strain curves of the ECAP-processed sample and aged samples, along with other properties listed in the table inset.

The samples corresponding to the peak aging were selected for TEM characterization, and the results are shown in Fig. 3a-d. Fig. 3a shows that the aged samples consists of equiaxed grains with

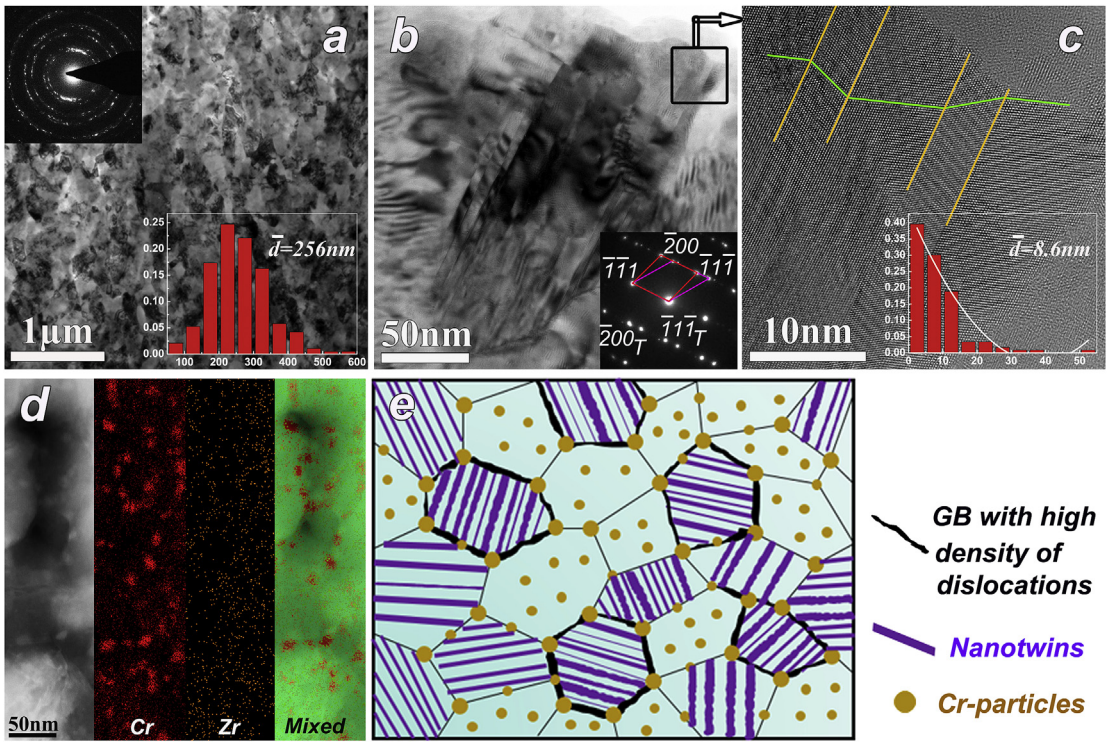

Fig. 3. The microstructures of CuCrZr alloy: (a) bright-field TEM image of a sample aged at 460 °C for 1.5 h, the insets are the corresponding SAED pattern and the grain size distribution; (b) the enlarged TEM image of a sub-micronsized grain from (a) containing nanotwins and the corresponding SAED pattern; (c) the HRTEM image of multiple twins from the boxed area in (b), and the statistical distributions for thickness of the T/M lamellae were obtained from the many TEM images of the same sample; (d) elemental map of the sample as the same as that for (a); (e) a schematic illustration of the multiscale architected structure composing of microstructures shown in (a–d).

random orientations (see the selected area electron diffraction pattern, SAED). The statistical results inserted in Fig. 1a show that more than 95% grains are smaller than 400 nm, with an average value of about 256 nm. One grain in (a) was enlarged along [110] orientation as shown in Fig. 3b, the grain contains a high density of nanotwins. The high-resolution TEM (HRTEM) image in the boxed area in Fig. 3b is displayed in Fig. 3c, which clearly shows multiple twins with thicknesses of few nanometers. At the end of the twins are high-density stacking faults.

The statistical results of the twin lamella thickness, from 300 such nanotwins embedded in 50 different sub-micronsized grains, are mostly distributed from several nanometers to dozens of nanometers. The twin lamella thickness distribution shows a peak at less than 5 nm, and the average lamellae thickness is approximately 8.6 nm for the edge-on twins. These special types of grains with sub-micrometer dimension, containing a high density of multiple twins with twin boundaries (TBs) spaced in the nanometer regime, are hereafter referred to as nanotwined ultrafine grains (UFGs). These nanotwined UFGs are ubiquitous in ECAP-processed and aged samples. Statistically, more than 65% grains are embedded with this architectured structure.

In ECAP-processed samples aged at 460 °C for 4 h, the elemental map in Fig. 3d demonstrates that most nanoscale Cr precipitates are located at the grain boundaries (GBs). Few precipitates were found in Twin/Matrix (T/M) lamella, which is different from the results reported by Li et al. [18]. The precipitates in the peak-aged sample are very small, beyond the resolution limit of the energy dispersive spectrometer (EDS). But according to the distribution of precipitates in over-aged sample, it is reasonable to assume that the precipitates in peak-aged samples are also mostly located at the boundaries of sub-micronsized grains.

4. Discussion

4.1. The formation of multiscale architected structure

Based on the above results, a sketch of microstructures in aged ECAP-processed samples corresponding to the microstructures shown in Fig. 3a–d, is given in Fig. 3e. It shows a general view of multiscale architected structure, composed of high popularity of nanotwined UFGs with Cr nano-precipitates at the GBs. An interesting strategy is demonstrated for strengthening and stabilizing the high conductive materials, UFGs containing nanoscale multiple twins providing strengthening and the nano-precipitates located on the GBs providing both strengthening and stabilization of the nanoscale structures.

In this work, the nanotwins are formed during plastic deformation and originated from GBs with high-density dislocations as shown as Fig. 4. These T/M lamellae is much thinner than those reported in Refs. [9,23], making them more difficult to be observed due to their weak contrast mixing with the strong contrast from high-density of stacking faults. They are only distinguishable in high-resolution TEM mode or under the weak beam conditions. It is understandable that there is no twins observed in Ref. [14] through ordinary bright-field TEM and selected area electron diffraction for multicrystal copper alloy. This nanotwined UFG structure are different from those reported by Lu et al. in Ref. [15]. Here, there are high-density of dislocations located at TBs (Fig. 4), typical of deformation twins [10,24]. However, in Ref. [15] most TBs were perfectly coherent and atomically sharp, typical of growth twins. It is also different from the single austenite phase with some remaining nanotwin bundles in the form of islands embedded in static recrystallization (SRX) grains reported in Refs. [9,23].

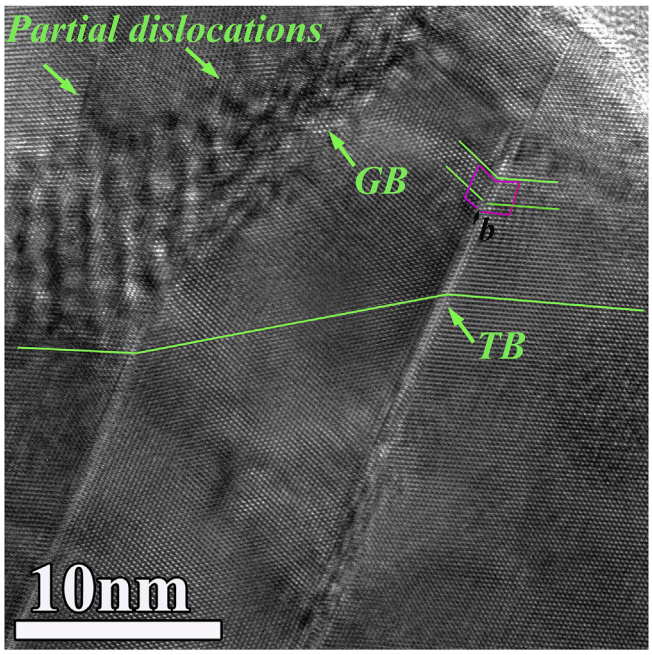

Fig. 4. Nanotwins formed via reaction of partial dislocations emitting from GB with high density of dislocations, the outlined area showing the presence of Shockley partial at theTB.

It was routinely believed that during ECAP, significant grain refinement occurs together with dislocation hardening, resulting in the significant enhancement of strength of a working material [14,25]. However, the high density of dislocations and GBs will lead to lower electrical conductivity [13] and thermal stability [26]. Obviously, it is easy to understand the high strength, but it is incomprehensible for the high electrical conductivity. It is known that the electrical resistivity of the coherent TBs is about one order of magnitude lower than that of conventional high-angle GBs [27]. With the addition of Cr and Zr, the stacking fault energy (SFE) of CuCrZr alloy becomes lower than that of pure Cu [28]. Lower SFE implies that the partial dislocations will be separated farther apart, which will induce more dislocation tangles to restrain dislocation movement because cross slip will be very difficult and even forbidden in some case [29]. With further straining, these dislocation tangles evolve into low angle GBs and act as dislocation sources, shown as Fig. 4. Low stacking fault energy also promotes twinning [30]. Twinning is orientation dependent. During ECAP, for the polycrystalline CuCrZr alloy with random orientations indicated in Fig. 3a, nanotwins may form only in a fraction of grains that possess favorable crystallographic orientations [9,31]. In the route B_c, the sample was rotated 90° every pass to change the strain paths, which significantly increases the twinning probability.

Cr precipitates prefer to form at the GBs of nanotwined UFGs, which would make sense in connection with the T/M lamellae thickness in samples here is in the same order as those of Cr precipitates, much less than that in room temperature rolled (average thickness of 87 nm) or cryo-rolled samples (average thickness of 48 nm) as reported in Ref. [18]. During aging, Cr atoms are easily to aggregate at TBs with low energy, due to the short diffusion distance (approximate to a half of T/M lamellae thickness). This diffusion distance to TBs is approximately the same as or even less than that for the forming of Cr precipitates. Cr atoms easily diffuse to TBs and then move to GBs along TBs. In other words, TBs serve as the passage for Cr atoms diffusion to GBs. If T/M lamellae is thicker, more Cr precipitates forming in twins [18]. As well as known, if the grain size decreases down to nanometer, there is no precipitate forming in the interior of gains [32]. By the same logic, it is well understood that there is no precipitate in the interior of nanotwins.

4.2. Strengthening mechanism

Generally, the yield stress (σ_{ys}) of alloys processed by SPD can be described as the sum of all calculated strengthening contributions in the following form:

$$\sigma_{ys} = \sigma_0 + K_H d^{-0.5} + \sigma_{SS} + \sigma_p + \sigma_D \quad (1)$$

where, σ_0 is the friction stress for pure Cu (= 36.5 MPa [13]), $K_H d^{-0.5}$ is the contribution from grain size, σ_{SS}, σ_p and σ_D are contributions from Cr solutes, Cr precipitates and stored dislocations calculated at the oneset of yield (0.2% strain), respectively. Note that σ_{SS} is quite low in peak- or over-aged sample, and thus can be neglected. In general, the contribution of precipitates (σ_p) can be estimated using the well-known Orowan bowing or shearing mechanism, depending on precipitate size and the nature of interface. These estimating methods are suitable for intragranular precipitate. However, in this work, most of precipitates locate on GBs (Fig. 5), it should consider the interaction between grain boundary glide and the Cr particles, rather than the interaction between gliding dislocations and the Cr particles. According to empirical relation, the stresses attributed to dislocation strengthening (σ_D) can be generally estimated by Kuhlmann-Wilsdorf mechanism [33]. In this work, we did not observe numerous forest dislocations in the grain interiors in the peak-aged ECAP samples, but a high density of dislocations at GBs and TBs. In this case, the stresses attributed to dislocation strengthening, estimated from Kuhlmann-Wilsdorf mechanism, are much higher than the experimental data. Actually, in this work it should give more consideration about the coupling relation between GBs/TBs and dislocations/precipitates, rather than the interaction between dislocations or and precipitates. However, at present there is no a suitable mechanism to assess the contribution from this coupling relation. For here, the best we can do is calculating the sum of contributions from these coupling relation according to Eq. (1) and the measured yield strength.

Considering the contribution from grain size (the second term in Eq. (1)), it must note there are two types of UFGs, as shown in Fig. 5, one is traditional UFG ($f_v = 35\%$) and the other is nano-twinned UFG ($f_v = 65\%$).

With traditional UFGs, the yield strength of metals can be expressed by Hall-Petch relationship [34]:

$$\sigma_{GB} = \sigma_0 + K_H d^{-0.5} \quad (2)$$

where, K_H is the Hall-Petch coefficient, d is the effective grain size calculated by the distance between any boundaries with a misorientation $\geq 2°$ [35,36]. As reported [13,37], $K_H = 0.129$ MPa $m^{0.5}$. According to the statistics in Fig. 3a, $d = 256$ nm. The σ_{GB} was calculated to be 291 MPa.

With nanotwined UFGs, the yield strength of metals follows the conventional Hall-Petch relationship with grain size replaced by average twin thickness λ [38]:

$$\sigma_{TB} = \sigma_0 + K_{TB}\lambda^{-0.5} \quad (3)$$

However, the above classical relationship breaks down when $\lambda < 15$ nm due to the softening caused by the preexisting Shockley partial dislocations at TBs (a natural phenomenon especially in deformation twins) [39,40]. The experimental yield strength for equiaxed grained nt-Cu samples with $\lambda = 8$ nm was determined to

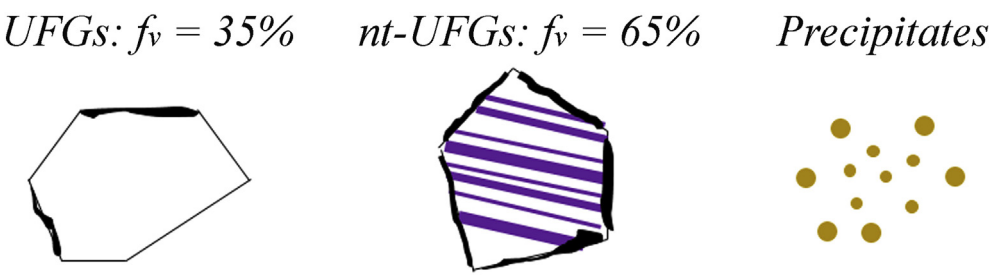

Fig. 5. Microstructure contributions to strengthening: UFGs, nano-twinned UFGs and precipitates.

be 550 MPa [39], it can be used here to estimate the strengthening from nt-UFGs.

Based on the above discussion and the rule-of-mixtures, Eq. (1) can be simplified in this work as:

$$\sigma_{ys} = \sigma_{GB} \times 35\% + \sigma_{TB} \times 65\% + \sigma_p + \sigma_D \quad (4)$$

where, the sum of the first two terms is about 459 MPa, the σ_{ys} of the peak-aged ECAP sample is 676 MPa, the strengthening contribution from Cr precipitates and dislocations is deduced to be 217 MPa.

4.3. The mechanism for high thermal stability and electrical conductivity

It is well accepted that a high thermal stability can be achieved in the UFG state of CuCrZr alloys subjected to severe plastic deformation, which is also confirmed by hardness measurement or differential scanning calorimetry (DSC) [14,41,42]. In this work, the thermal stability of the UFG structure was characterized by hardness and grain size. The grain size monitor is also used to study the thermal stability of ultrafine grained copper [43]. Fig. 1a shows that no grain growth during annealing under 500 °C for 1 h, mainly due to GBs with low energy and also nanometer-sized Cr precipitates at the GBs blocking the motion of GBs. The solubility of Cr in Cu varies from 0.05 wt% at 500 °C to 0.27 wt% at 1000 °C [44], the grain coarsening and hardness decreasing at the temperature above 500 °C is partially due to dissolution of Cr-particles.

As well known that the electrical conductivity of Cu alloys is lower than 80% IACS, depending upon the alloy content and the state of being. The electrical conductivity of ECAPed CuCrZr alloy is low in Fig. 1b because of the supersaturated Cr in Cu. The electrical conductivity recovers significantly at the early stage of aging due to Cr precipitation. After 1 h, electrical conductivity recovers to 70.7% IACS, and then keeps going up though slightly slower, reaches to 83.1% IACS at 8 h. Besides the contribution of Cr precipitation, deformation-induced defects (dislocations and vacancies) annihilation during annealing is also helpful. Additionally, boundaries also influence the electrical conductivity of alloy. Researches indicate that the intrinsic GBs resistivity of Cu will increase 2×10^{-7} nΩ m^2 with GB misorientations from low to high angles [17]; the electrical resistivity of TBs is usually considered to be half of the specific stacking fault resistivity, much lower than those of conventional GBs [15]; numerous dislocations accumulating at the TBs have a negligible influence on the specific TB resistivity [45]. Consequently, the deformation TBs is helpful to increasing the overall electrical conductivity.

5. Conclusions

In summary, a novel multiscale architectured structure, i.e., nanotwined UFGs surrounded by nano-precipitates, was observed in aged ECAP-samples in a CuCrZr alloy. It produced a superior combination of strength, electrical conductivity and thermal stability in the alloy. This provides insight understanding on the mechanisms for strengthening, thermal stability and electrical conductivity, and could help the development of high-performance electrical conductors.

Acknowledgments

This work was funded by the National Key R&D Program of China (No. 2017YFA0204403), the National Natural Science Foundation of China (No. 51301064), MOST of China (2012CB932203), and the Fundamental Research Funds for the Central Universities (Grant No. 30915012104). The authors are grateful to Dr. Z.S. You for his assistance with discussions about the strengthening mechanism. All TEM experiments were performed at the Materials Characterization and Research Center of Nanjing University of Science and Technology.

References

[1] I.S. Batra, G.K. Dey, U.D. Kulkarni, S. Banerjee, J. Nucl. Mater. 299 (2) (2001) 91–100.
[2] Q. Liu, X. Zhang, Y. Ge, J. Wang, J.-Z. Cui, Metall. Mater. Trans. A 37 (11) (2006) 3233–3238.
[3] Y. Amouyal, S.V. Divinski, Y. Estrin, E. Rabkin, Acta Mater. 55 (17) (2007) 5968–5979.
[4] G. Ghosh, J. Miyake, M.E. Fine, JOM 49 (3) (1997) 56–60.
[5] A. Vinogradov, Y. Suzuki, T. Ishida, K. Kitagawa, V.I. Kopylov, Mater. Trans. JIM 45 (7) (2004) 2187–2191.
[6] K. Lu, Nat. Rev. Microbiol. 1 (2016) 16019.
[7] J.Z. Liu, J.H. Chen, D.W. Yuan, C.L. Wu, J. Zhu, Z.Y. Cheng, Mater. Char. 99 (2015) 277–286.
[8] J.Z. Liu, J.H. Chen, Z.R. Liu, C.L. Wu, Mater. Char. 99 (2015) 142–149.
[9] K. Lu, F.K. Yan, H.T. Wang, N.R. Tao, Scripta Mater. 66 (11) (2012) 878–883.
[10] Y.T. Zhu, X.Z. Liao, X.L. Wu, Prog. Mater. Sci. 57 (1) (2012) 1–62.
[11] Y.T. Zhu, X. Liao, Nat. Mater. 3 (6) (2004) 351–352.
[12] Y.T. Zhu, T.G. Langdon, Mater. Sci. Eng. A 409 (1–2) (2005) 234–242.
[13] R. Mishnev, I. Shakhova, A. Belyakov, R. Kaibyshev, Mater. Sci. Eng. A 629 (2015) 29–40.
[14] A. Vinogradov, V. Patlan, Y. Suzuki, K. Kitagawa, V.I. Kopylov, Acta Mater. 50 (7) (2002) 1639–1651.
[15] L. Lu, Y. Shen, X. Chen, L. Qian, K. Lu, Science 304 (5669) (2004) 422–426.
[16] Y. Zhang, Y.S. Li, N.R. Tao, K. Lu, Appl. Phys. Lett. 91 (21) (2007), 211901.
[17] L.X. Sun, N.R. Tao, K. Lu, Scripta Mater. 99 (2015) 73–76.
[18] R. Li, H. Kang, Z. Chen, G. Fan, C. Zou, W. Wang, S. Zhang, Y. Lu, J. Jie, Z. Cao, T. Li, T. Wang, Sci. Rep. 6 (2016), 20799.
[19] A.P. Zhilyaev, A. Morozova, J.M. Cabrera, R. Kaibyshev, T.G. Langdon, J. Mater. Sci. 52 (1) (2017) 305–313.
[20] G. Purcek, H. Yanar, M. Demirtas, Y. Alemdag, D.V. Shangina, S.V. Dobatkin, Mater. Sci. Eng. A 649 (2016) 114–122.
[21] A. Hernández-Pérez, M. Eddahbi, M.A. Monge, A. Muñoz, B. Savoini, Fusion Eng. Des. 98–99 (2015) 1978–1981.
[22] Y.T. Zhu, T.C. Lowe, Mater. Sci. Eng. A 291 (1–2) (2000) 46–53.
[23] H.T. Wang, N.R. Tao, K. Lu, Acta Mater. 60 (9) (2012) 4027–4040.
[24] J.W. Christian, S. Mahajan, Prog. Mater. Sci. 39 (1) (1995) 1–157.
[25] R.Z. Valiev, R.K. Islamgaliev, I.V. Alexandrov, Prog. Mater. Sci. 45 (2) (2000) 103–189.
[26] Y. Estrin, A. Vinogradov, Acta Mater. 61 (3) (2013) 782–817.
[27] A.P. Sutton, R.W. Balluffi, Interfaces in Crystalline Materials, Clarendon, Oxford, 1995.

[28] K. Kapoor, D. Lahiri, I.S. Batra, S.V.R. Rao, T. Sanyal, Mater. Char. 54 (2) (2005) 131–140.
[29] H. Feng, H. Jiang, D. Yan, L. Rong, Mater. Sci. Eng. A 582 (2013) 219–224.
[30] R.Z. Valiev, Y. Estrin, Z. Horita, T.G. Langdon, M.J. Zehetbauer, Y.T. Zhu, Mater. Res. Lett. 4 (1) (2016) 1–21.
[31] C.S. Hong, N.R. Tao, X. Huang, K. Lu, Acta Mater. 58 (8) (2010) 3103–3116.
[32] P.V. Liddicoat, X.-Z. Liao, Y. Zhao, Y. Zhu, M.Y. Murashkin, E.J. Lavernia, R.Z. Valiev, S.P. Ringer, Nat. Commun. 1 (2010) 63.
[33] D. Kuhlmann-Wilsdorf, Mater. Sci. Eng. A 113 (Supplement C) (1989) 1–41.
[34] R.W. Armstrong, Mater. Trans. 55 (1) (2014) 2–12.
[35] N. Kamikawa, X. Huang, N. Tsuji, N. Hansen, Acta Mater. 57 (14) (2009) 4198–4208.
[36] S. Malopheyev, R. Kaibyshev, Mater. Sci. Eng. A 620 (2015) 246–252.
[37] K.V. León, M.A. Muñoz-Morris, D.G. Morris, Mater. Sci. Eng. A 536 (2012) 181–189.
[38] Z.S. You, L. Lu, K. Lu, Acta Mater. 59 (18) (2011) 6927–6937.
[39] L. Lu, X. Chen, X. Huang, K. Lu, Science 323 (5914) (2009) 607–610.
[40] L. Lu, Z.S. You, K. Lu, Scripta Mater. 66 (11) (2012) 837–842.
[41] A. Vinogradov, Y. Suzuki, T. Ishida, K. Kitagawa, V.I. Kopylov, Mater. Trans. 45 (7) (2004) 2187–2191.
[42] P.K. Jayakumar, K. Balasubramanian, G. Rabindranath Tagore, Mater. Sci. Eng. A 538 (Supplement C) (2012) 7–13.
[43] O. Man, L. Pantvlejev, L. Kunz, Mater. Trans. 51 (2) (2010) 209–213.
[44] D.J. Chakrabarti, D.E. Laughlin, Bull. Alloy Phase Diagrams 5 (1) (1984) 59–68.
[45] X.H. Chen, L. Lu, K. Lu, J. Appl. Phys. 102 (8) (2007), 083708.